Reliability analysis of low-voltage metal-oxide surge arresters using accelerated failure time model

Pitshou Bokoro, *Member, IEEE,* Wesley Doorsamy, *Member, IEEE,*

***Abstract*—Failure progression of metal oxide-based surge arresters in response to exposure to harmonics is modelled using the accelerated failure time model. Multi-stress accelerated ageing tests, with and without AC distorted voltage stress, are conducted on arrester samples sourced from different suppliers to obtain baseline and harmonic-factor logarithmic life and reliability functions. A maximum likelihood approach is taken to estimating the accelerated failure time model parameters based on the failure time data. The modelled harmonic-factor reliabilities prove MOV life acceleration and show multiplicative failure progression of up to 41 times faster for a THD content of 8.52% in the applied voltage stress.**

***Index Terms*—Accelerated failure time, metal oxide surge arrester, accelerated multi-stress ageing, reliability, life.**

I. Introduction

CONTINUOUSLY applied ac or dc voltage stress to metal oxide surge arresters (MOSA) may increase conduction level of thermally stimulated currents (TSC) through these surge protection devices (SPDs) [1] – [3]. This phenomenon is reported to be one of the triggers or major causes of degradation-based failure mode, which negatively impacts on the reliability and useful life of varistor-based SPDs [4] – [6]. Reduced life and/or reliability of MOSA devices has proven to be aggravated if the constantly applied voltage stress consists of harmonic frequencies [7] , [8]. The major shortcoming in this finding remains the non-existence of supporting model which may be relied upon in order to predict the accelerating or reduction effect of harmonic distortion stresses on time to failure (t_j) and therefore on reliability $[R(t_j)]$ of MOSA devices.

In this work, an accelerated failure time (AFT) model is proposed to predict the progression factor of degradation-based failure affecting metal oxide varistors (MOV) arresters when subjected to the following stresses: fundamental voltage component, harmonic voltage component and thermal. Therefore, two sets of low-voltage MOSA sourced from three different manufacturers are tested using standard accelerated life tests. A continuous voltage stress (with and without) distortion is used to enable current conduction through the test samples at constant temperature of 135^{o}C for a test period of 96 hours. The failure times observed and recorded during experimental tests are treated in accordance with the IEEE guide for statistical analysis of solid insulation breakdown [9]. The AFT model is then used to examine the progression factor that influences reliability and life functions as a result of harmonics. Results obtained indicate a baseline up to 41 times greater than the AFT reliability for 8.52% THD content.

P. Bokoro and **W. Doorsamy** are both senior lecturers in the Department of Electrical and Electronic Engineering Technology, University of Johannesburg, South Africa.

II. Multi-stress accelerated ageing of MOSA

The synergistic effects of various forms of stress (thermal, electrical, radiation...) on insulators and dielectrics of power system equipment are reported to be fundamental triggers of ageing or degradation [10] – [14]. Electrical and thermal stresses are simultaneously encountered in the operation of metal oxide-based surge arresters (MOSA) [15], [16]. This raises the need for simulating electro-thermal stress for the purpose of reliability studies of metal oxide surge arresters (MOSA) devices. The combined effect of these stresses is conventionally simulated at faster rates using accelerated ageing or life tests [17], [18]. However, electrical stress such as generally contemplated in accelerated ageing or life tests assumes constantly or progressively applied DC or sinusoidal AC voltage waveform (fundamental) [19], [20]. Yet, the increased use of power electronics devices in modern power networks has significantly influenced the quality of voltage and/or current waveform likely to be available in electrical circuits. Additional harmonic frequencies, if present in the voltage stress applied to MOSA, have reportedly proven to have some degree of influence on condition monitoring techniques as well as on the reliability of metal oxide-based surge arresters [7], [8], [21], [22]. Simulation of combined effects of simultaneously applied distorted-voltage and thermal stresses on metal oxide-based surge arresters has been demonstrated in [7], [8]. Harmonic voltages are generated on the basis of interaction between circulating non-linear currents, created as a result of one or more power electronics components connected across arrester samples, and the impedance of the source [23], [24].

III. Experimental Work

A. Accelerated Ageing Test

Accelerated electro-thermal ageing of MOSA devices was experimentally designed using the Nabertherm P330 heat chamber, the TDGC$_2$ 50 Hz AC variable voltage source and a triac-based AC voltage controller to ensure continuously-applied distorted AC voltage and thermal stresses. The heat chamber was set to execute a heating program consisting of three ramp and three holding times before settling at a constant temperature of 135^{o}C was achieved for a test period of 96 hours. The magnitude of continuously applied fundamental AC

voltage stress was fixed at 85 % of varistor samples' reference voltage (V_{1mAAC}). The triac-based AC voltage controller was continuously switched on to supply a resistive-inductive load when harmonic voltage stresses were required. The percentage content of harmonic frequencies generated in each test case observed is summarised in table I.

TABLE I
PERCENTAGE CONTENT OF HARMONIC FREQUENCIES GENERATED

Samples	V_{1mAAC}	0.85 V_{1mAAC}	3^{rd}	5^{th}	7^{th}	THD
Case 1	205	175.25	6.24	5.58	6.63	10.68
Case 2	200	170	9.8	6.9	5.8	13.32
Case 3	228	193.8	4.5	5.5	4.7	8.52
Units	V	V	%	%	%	%

The voltage source was time-delayed in order to accommodate thermal transient related to ramp and holding times of the heating program to settle. This enabled synchronisation between distorted voltage and thermal stresses. High temperature conductors (1.5 mm^2 Silflex) were used to connected the TDGC$_2$ 50 Hz supply voltage source to each of the five arrester samples mounted in parallel configuration inside the chamber for each test-run conducted. Each of parallel sub-circuits was protected against short circuits using a 125 mA slow-blow fuse. The data acquisition system used to capture the times to failure (t_j) consisted of three-channel K5020 and MT250 data-loggers. The multi-stress accelerated ageing test conducted in this work is shown in figure 1. Therefore, accelerated ageing

Fig. 1. Multi-stress accelerated ageing test

test such as performed in this work consisted of six cases involving three sample groups namely: BL, YW and RD. Each group consisted of 120 sample units of which one half was tested with harmonics and the other without.

B. Failure criteria, Data Censoring and Weibull Fitness Test

1. Failure Criteria and Data Censoring: In each of the test cases conducted in this study, the time to failure of the tested device, such as recorded by data acquisition equipment, was defined as the time-period between two major events: the start of conduction through varistors and short-circuit interruption by a protective fuse. In order to rule out any probability of short-circuit resulting from any reason other than varistor degradation, change in the DC reference voltage (ΔV_{1mADC}) of the samples was verified before and after accelerated ageing testing in order to ensure that degradation-based failure has occurred. The following failure criteria was therefore applied:

$t_j \leq 96\ hours$ and $\Delta V_{1mADC} \geq 5\%$: Failed
$t_j = 96\ hours$ and $\Delta V_{1mADC} < 5\%$: Survived
$t_j < 96\ hours$ and $\Delta V_{1mADC} < 5\%$: Spoiled

As a result of accelerated ageing procedure, times to failure data thus obtained were extrapolated using the following relationship [16, 17]:

$$\hat{t_j} = t_j \times 2.5^{\frac{(T_t - 40)}{10}} \tag{1}$$

Where:

$\hat{t_j}$: is the extrapolated failure time
t_j: is the actual measured failure time
T_t: is the test temperature

The number of MOSA samples that were registered as failed (denoted as r) in each of the test cases conducted are shown in table II.

TABLE II
NUMBER OF FAILED SAMPLES PER GROUP

Sample Groups	with harmonics (r)	without harmonics (r)
BL	37	27
YW	47	36
RD	56	41

2. Weibull Fitness Test and Estimation of Parameters: The Weibull statistical distribution is usually adequate to times to failure of life data [25]-[27]. The fitness of the data obtained in each of the cases examined in this work can be tested using the correlation factor. Prior to this, the percentage cumulative probability is determined using Ross approximation [28]:

$$F(j,n) \approx \left(\frac{j - 0.44}{n + 0.25}\right) \times 100 \tag{2}$$

Where:

$F(j,n)$: is the cumulative failure probability
j: is the failure ranking
n: is the number of samples

The correlation factor $C(p_j, q_j)$ can therefore be obtained using the following function:

$$C(p_j, q_j) = \frac{\sum (p_j - \overline{p}) \cdot (q_j - \overline{q})}{\sqrt{\sum (p_j - \overline{p})^2 \cdot \sum (q_j - \overline{q})^2}} \tag{3}$$

Where each probability of failure is assigned a value expressed as a percentage:

$$p_j = \ln\left[-\ln\left(1 - \frac{F(j,n)}{100}\right)\right] \tag{4}$$

$$\overline{p} = \frac{\sum p_j}{r} \tag{5}$$

And each breakdown time is assigned a value:

$$q_j = \ln\left(\hat{t_j}\right) \tag{6}$$

$$\overline{q} = \frac{\sum q_j}{r} \tag{7}$$

For fitness purpose, the calculated correlation factor should be equal or higher than the critical coefficient value $[C_{critical}\,(p_j, q_j)]$ [28]:

$$C\,(p_j, q_j) \geq C_{critical}\,(p_j, q_j)$$

Subsequent to the fitness test, the Weibull parameters (shape and scale) can be estimated using least squares regression techniques. This method suggests that the both the shape and the scale parameters be determined on the basis of the slope and the intercept of the cumulative distribution function (CDF) such as obtained from $\left[\hat{t_j}, F\,(j,n)\right]$ points [28]. The slope $m\,(p_j, q_j)$ and the intercept are determined using the following relations, respectively:

$$m\,(p_j, q_j) \;\; = \frac{\sum (p_j - \overline{p}) \cdot (q_j - \overline{q})}{\sum (p_j - \overline{p})^2} \tag{8}$$

And:

$$Intercept = \overline{q} - m\,(p_j, q_j) \tag{9}$$

The shape parameter (β) can be estimated using the reciprocal of the slope. This leads to the following relation:

$$\beta = \frac{1}{m\,(p_j, q_j)} = \frac{\sum (p_j - \overline{p})^2}{\sum (p_j - \overline{p}) \cdot (q_j - \overline{q})} \tag{10}$$

The scale parameter (α) may be obtained using the exponential of the intercept:

$$\alpha = \exp\left[\overline{q} - m\,(p_j, q_j)\right] \tag{11}$$

C. Experimental Results

The $\left[\hat{t_j}, F\,(j,n)\right]$ data-points obtained from equations (1) and (2) are used to plot the CDF curves which are further tested for fitness to the Weibull distribution. The CDF curves obtained for all sample groups tested without and with harmonics are given in figures 2, 3 and 4. However the adequacy of the resulting CDF curves or the fitness of the distributions obtained to the Weibull is verified by substituting the p_j and q_j, obtained from equations (4) and (6) as well as $\overline{p}$ and $\overline{q}$ from (5) and (7), into equations (3), (8), (9), (10) and (11) for the purpose of computing respective correlation factors and subsequently the shape and scale parameters. These results are summarised in table III and show adequacy of the distributions to the Weibull. Moreover, the CDF curves demonstrate higher probability of ageing when subjected to thermal and AC distorted voltage stresses. The Weibull probability density function (PDF) $f\,(t, \beta, \alpha)$, which reveals both the reliability and failure rate or hazard functions could be relied upon in order to analyse further the behaviour of MOSA samples under thermal and AC distorted stresses.

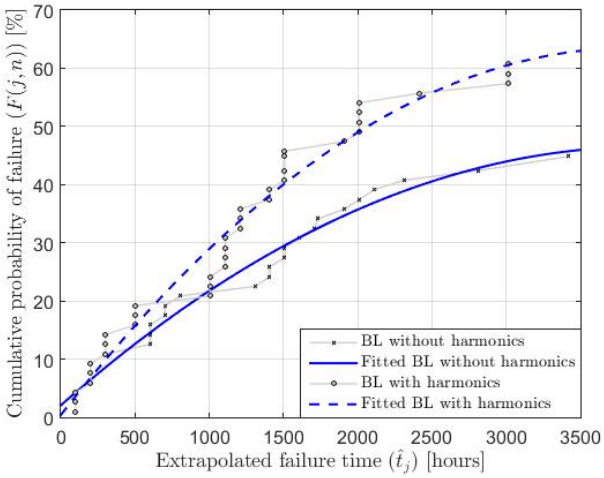

Fig. 2. CDF curves: BL without and with harmonics

The Weibull PDF $\left[f\left(\hat{t_j}, \beta, \alpha\right)\right]$ is expressed in terms of the reliability $R(\hat{t_j})$ and failure rate or hasard $h(\hat{t_j})$ functions. This is expressed using the following equation:

$$f\left(\hat{t_j}, \beta, \alpha\right) = \frac{\beta}{\alpha} \cdot \left(\frac{\hat{t_j}}{\alpha}\right)^{\beta-1} \cdot \exp\left(-\frac{\hat{t_j}}{\alpha}\right)^{\beta} \quad \hat{t_j} \geq 0 \tag{12}$$

Where:

$$\exp\left(-\frac{\hat{t_j}}{\alpha}\right)^{\beta} = R\left(\hat{t_j}\right) \tag{13}$$

And:

$$\frac{\beta}{\alpha} \cdot \left(\frac{\hat{t_j}}{\alpha}\right)^{\beta-1} = h\left(\hat{t_j}\right) \tag{14}$$

TABLE III
CORRELATION FACTORS, SHAPE AND SCALE PARAMETERS OBTAINED

With Harmonics	$C\,(p_j, q_j)$	$C_{critical}\,(p_j, q_j)$	β	α
BL	0.955857	≈ 0.95	1.093	2746.5
YW	0.951579	≈ 0.95	1.71	726.68
RD	0.974395	≈ 0.96	1.8	765.22
Without Harmonics	$C\,(p_j, q_j)$	$C_{critical}\,(p_j, q_j)$	β	α
BL	0.958317	≈ 0.94	0.98	4167.6
YW	0.935602	≈ 0.94	1.46	1103.3
RD	0.969156	≈ 0.95	1.63	1079.4

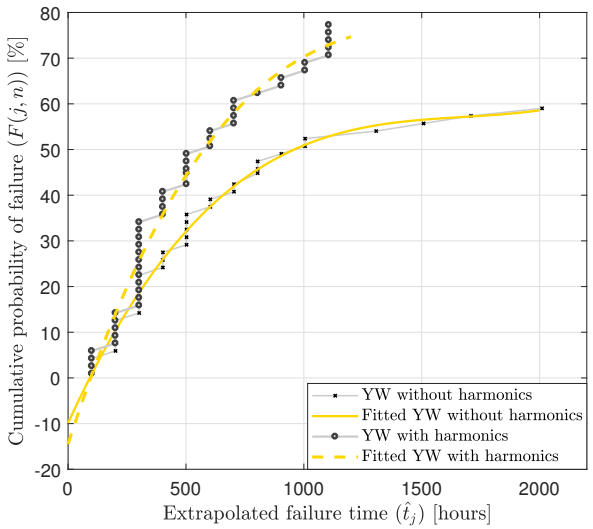

Fig. 3. CDF curves: YW without and with harmonics

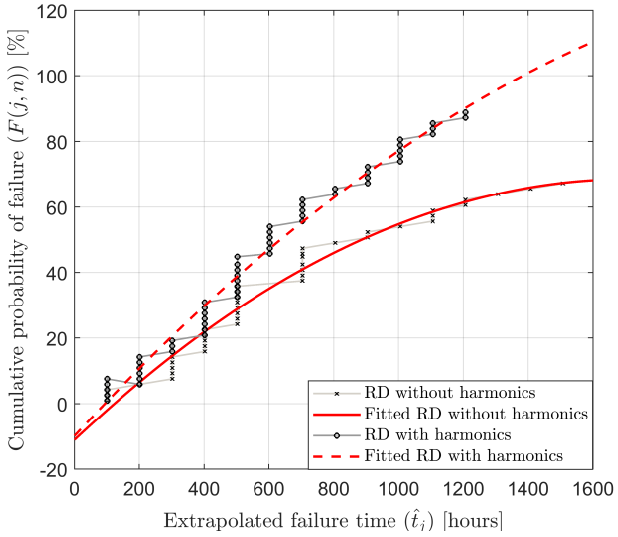

Fig. 4. CDF curves: RD without and with harmonics

The reliability curves for each of the three sample cases are shown in figures 5, 7 and 9. Hazard curves are shown in figures 6, 8 and 10. It suggests lower reliability across the observed time-points for samples subjected to thermal and distorted AC voltage stress. The shape of the Hazard curves in figures 6, 8 and 10 give some additional insight into MOV failure mechanisms. It is observed that MOVs tend to have a high infant mortality rate with a larger portion failing during the first 100 hours of the accelerated ageing test regardless of the presence of the harmonic stress. This change in hazard rate forms a dog-leg shape and is indicative of a device with several failure modes [29], which is consistent with the previously mentioned literature on MOV failure mechanisms. Similarly for the failure rate curves, higher failure rate across the observed time-points could be noticed for samples under thermal and distorted AC voltage stress.

Therefore, the experimental results thus discussed fundamentally suggest life or time to failure reduction of MOSA devices as a result of AC distorted voltage stress. The AFT model is therefore applied in an attempt to model life reduction as a result AC distorted voltage stress.

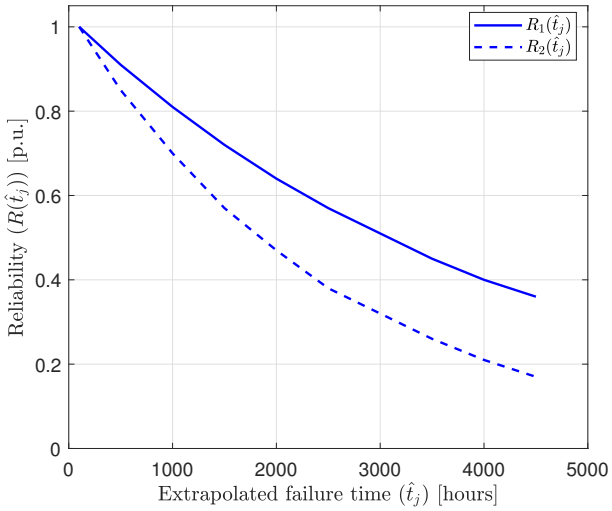

Fig. 5. Reliability curves: BL without and with harmonics

IV. ACCELERATED FAILURE TIME MODEL

AFT model is commonly used for the purpose of analysing or predicting the relationship between survival data and the covariates or predictors [30]. It is mostly found to be applied in various fields such as medical and pharmaceutical research as well as in manufacturing and industrial applications [31], [32]. Survival or reliability data such as used in this model should be

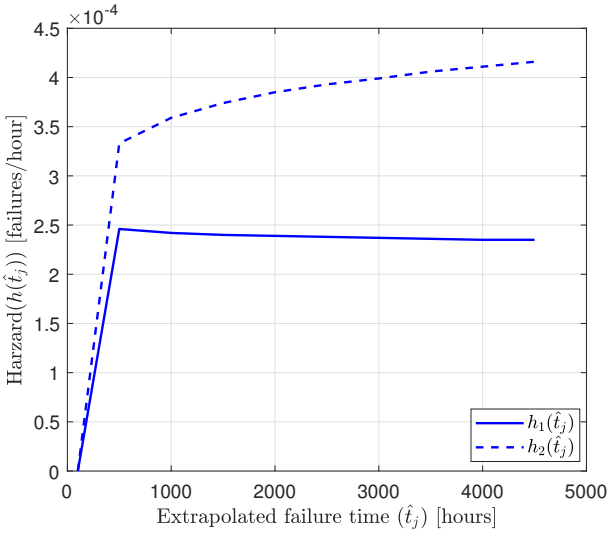

Fig. 6. Failure rate curves: BL without and with harmonics

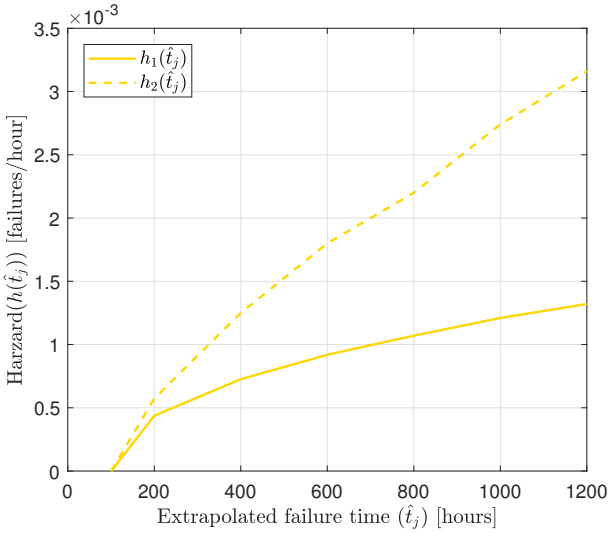

Fig. 8. Failure rate curves: YW without and with harmonics

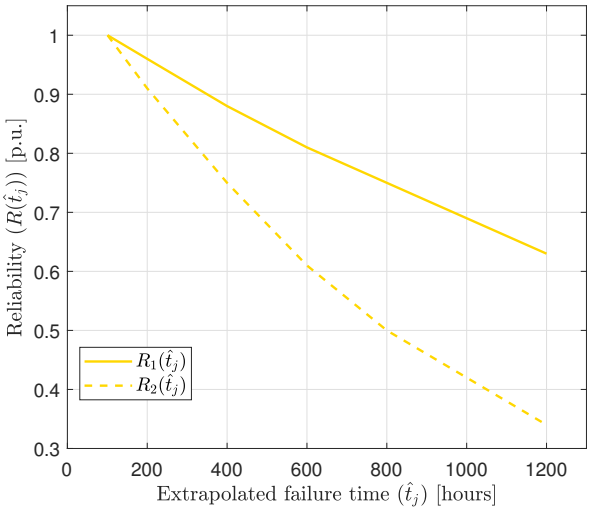

Fig. 7. Reliability curves: YW without and with harmonics

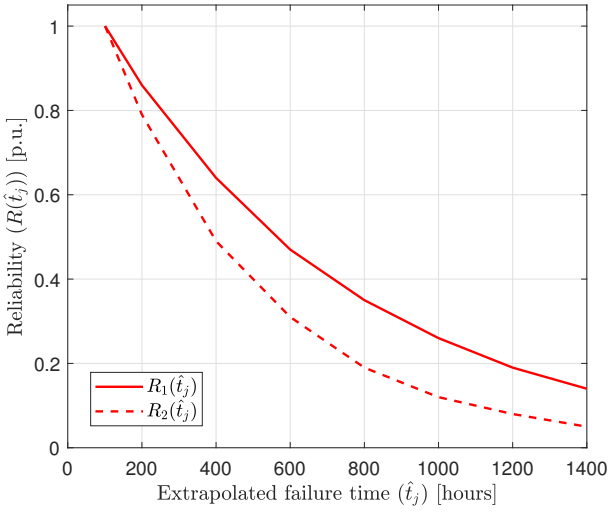

Fig. 9. Reliability curves: RD without and with harmonics

identified to fit a particular statistical distribution (exponential, Weibull and gamma) [33]. Therefore, the contributing effect of harmonics-distortion on reliability of MOV devices, such as experimentally demonstrated, could be modelled using AFT technique. The direct effect of covariates on the survival or reliability baseline of MOSA is expressed as follows [33, 34]:

$$R\left(t_j|X\right) = \exp\left(-\frac{t_j}{\alpha}\right)^{\beta} \cdot \exp\left(bX\right) \tag{15}$$

Where:

$R(t_j|X)$: AFT reliability function.
$\exp(-\frac{t_j}{\alpha})^{\beta}$: baseline reliability function.
$\exp(bX)$: the accelerating or reduction factor.

A logarithmic-linear transformation of equation (15) yields the log-linear expression of the AFT model which expresses the effect of a covariate or a predictor to the failure time of MOV devices. This is given as follows :

$$\ln t_j = \mu + bX + \alpha \cdot \epsilon_j \tag{16}$$

Where:

$\ln t_j$: log value of time to failure at rank j.
μ : is the intercept.
b : is AFT regression coefficient.
X : is a covariate or predictor.
α : is the scale parameter.
ϵ_j : is the random error.

The accelerating factor is fundamentally dependent on two states of the covariates or predictors: No harmonics $(X = 0)$ and with harmonics $(X = 1)$.

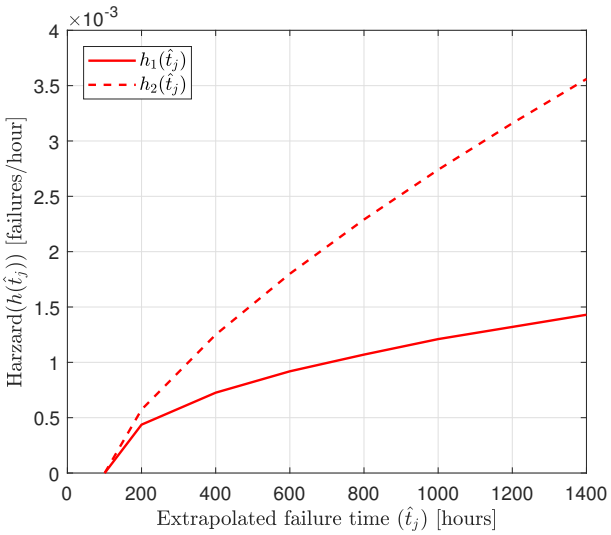

Fig. 10. Failure rate curves: RD without and with harmonics

V. Estimation of the AFT Model Parameters

The maximum likelihood estimates of the regression coefficient, the intercept and the scale factor $L\,(b, \mu, \alpha)$ is obtained by performing accelerated failure time regression using the Matlab AFT routine which is essentially similar to the SAS survreg routine [35]:

$$L\,(b, \mu, \alpha) = \prod_{j=1}^{n} \{f_j(t_j)\}^{\delta_j} \cdot \{R(_j)\}^{1-\delta_j} \qquad (17)$$

Where:

$f_j(t_j)$: is the density function.
$R(t_j)$: is the reliability function.
δ_j : is the event indicator.

The AFT routine used maximises the likelihood by setting the partial derivatives of the given log-likelihood equation indicated in (16) to zero. The resulting set of equations are then solved using the approach of a typical constrained optimisation problem. Since there is only one indicator $(X = 1)$ for the condition of harmonics, there is only one regression coefficient b to be determined. The predictor $(X = 0)$ only when there is application of mains without external harmonics and is used as a baseline indicator for the model. In the baseline case, the AFT model reverts to the standard survival distribution as given by equation (13). The estimates $\hat{\mu}$, $\hat{b}$ and $\hat{\alpha}$ that minimise the log-likelihood and maximise the likelihood using the failure times for each sample group are given in Table IV. It should be noted that a negative value of the regression coefficient implies life acceleration or reliability reduction while a positive value indicates life deceleration or enhanced reliability [36], [37]. The resulting z-scores, p-values and standard errors are provided in table IV. The z-scores and p-values are test statistics that provide information about the significance of the AFT factor i.e. harmonics. The resulting high values of z and low p-values i.e. $|z|>$ 1.96 and $p<$ 0.05 with 95% confidence interval, indicate that the AFT factor (X) or influence of harmonics on MOV reliability is statistically significant. The overview of the methodology followed in this paper is shown in figure 11.

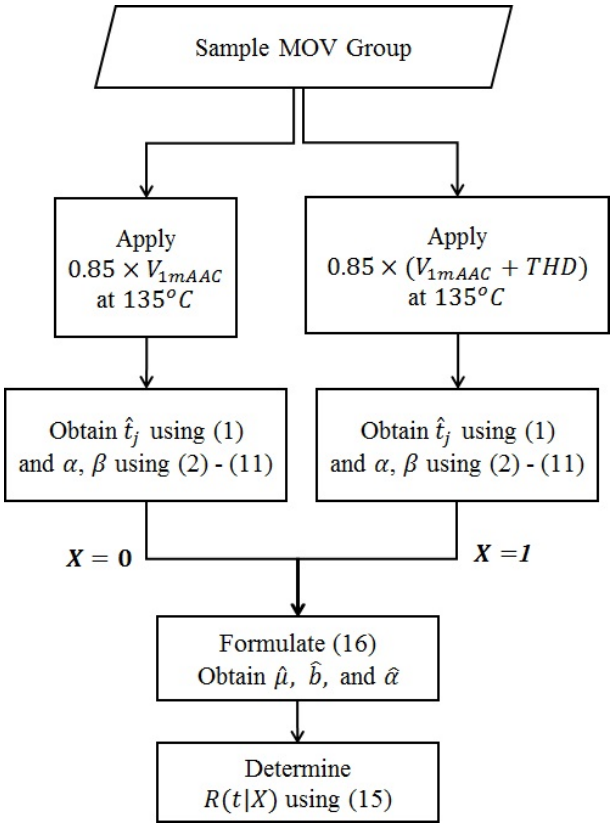

Fig. 11. Overview of AFT methodology

VI. Results and Discussion

For the three cases observed in this study, the estimated value for the regression coefficient $\hat{b}$ is computed to be: -2.89531 for BL samples, -1.92106 for YW samples, and -3.71373 for RD samples. These values quantify the reduction in life and reliability, due to harmonics, that were initially observed in figures 5, 7 and 9. The extent to which the baseline reliability or time to failure is directly affected by distorted voltage stress is determined using (15). Therefore, the life reduction factor is found to be: 0.055 for BL samples; 0.146 for YW samples; and 0.024 for RD samples. This suggests that a THD content of 10.68% in the applied voltage stress accelerates life by approximately 18 times for the BL samples. Similarly, the accelerated life is 6.8 times faster than the baseline for YW samples for a THD content of 13.32 %, and 41 times faster for RD samples for a THD content of 8.52%.

Observing the behaviour of the AFT reliabilities shown in figure 11, as obtained from equation (15), during the time-interval $[1, 10000]$ hours, it could be noted that: despite having the least percentage harmonic content in the voltage stress, RD samples show the worst reliability curve while YW samples demonstrated the best reliability behaviour before $\hat{t_j}$ = 1000 hours, despite being stressed with the highest THD

TABLE IV
AFT PARAMETER ESTIMATES

BL Samples					
Parameters	Estimates	Standard Error (SE)	95% Confidence Intervals	Z-scores	p-values
$\hat{\mu}$	14.7674	0.96488	12.8762 16.6585	15.3049	7.09×10^{-53}
$\hat{b}$	− 2.89531	1.22724	−5.30069 − 0.48992	−2.35921	0.0183
$\ln \hat{t_j}$	1.56495	0.10732	1.35461 1.77528	14.5827	0
$\hat{\alpha}$	4.78242	0.51323	3.87524 5.90196		
$L(b,\mu,\alpha)$	− 249.701				
YW Samples					
Parameters	Estimates	Standard Error (SE)	95% Confidence Intervals	Z-scores	p-values
$\hat{\mu}$	10.3066	0.65296	9.02682 11.5864	15.7844	3.98×10^{-53}
$\hat{b}$	−1.92106	0.86651	−3.61942 −0.22271	− 2.21702	0.0266
$\ln \hat{t_j}$	1.36339	0.08189	1.20288 1.5239	16.6488	0
$\hat{\alpha}$	3.90942	0.32015	3.3297 4.59007		
$L(b,\mu,\alpha)$	−263.216				
RD Samples					
Parameters	Estimates	Standard Error (SE)	95% Confidence Intervals	Z-scores	p-values
$\hat{\mu}$	10.4756	0.46987	9.55464 11.3965	22.2948	4.148687×10^{-110}
$\hat{b}$	−3.71373	0.60999	−4.90931 −2.51815	−6.08819	1.14194×10^{-9}
$\ln \hat{t_j}$	1.08649	0.07413	0.94119 1.23178	14.6569	0
$\hat{\alpha}$	2.96384	0.2197	2.56304 3.42731		
$L(b,\mu,\alpha)$	−271.673				

content. This phenomenon could be attributed to differences in manufacturing processes and chemical additives in the microstructure of these arrester devices. The AFT reliability curves are shown in figure 12.

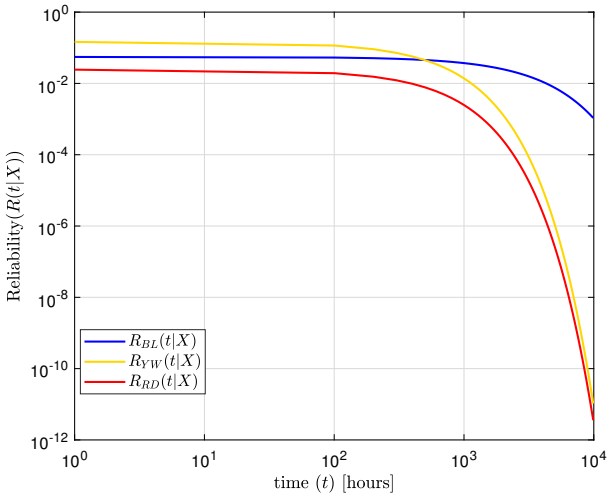

Fig. 12. AFT Reliability curves

VII. CONCLUSION

The AFT model is used in this study in order to evaluate the degree or extent in which times to failure or reliability function of MOV-based surge arresters are accelerated or reduced as a result of distorted AC voltage stress. Failure times data obtained from accelerated multi-stress ageing test conducted on three samples groups are used to generate baseline reliability. The unicovariate AFT model applied yields the following observations:

1) The AFT model consists of an adequate technique that could be used by both manufacturers and consumers in order to predict the effect of one or many other factors on the reliability of MOV-based surge arresters and thereby ensuring the quality of surge protection to be expected under any given applied stress conditions.

2) Higher or lower content of THD in the applied AC distorted voltage stress may not necessarily trigger higher or lower influence on MOV failure trends or poor performance reliability.

3) Resilience to AC distorted voltage stress, owing to differences in manufacturers' sintering processes and chemical composition of MOV microstructure, may change patterns (high or low resilience) at any point in time during the failure process.

ACKNOWLEDGMENT

The authors would like to express their sincere thanks to the Tertiary Education Support Programme (TESP) of the South African power utility company for their continued support.

REFERENCES

[1] M. Wang, Q. Tang, and C. Yao. *Electrical properties and AC degradation characteristics of low voltage ZnO varistors doped with* Nd_2O_3. Ceramics International, Vol.36, no.3, pp.1095-1099, January 2010.

[2] J. He, J. Liu, J. Hu, and W. Long. *AC ageing characteristics of* Y_2O_3*-doped ZnO varistors with high voltage gradient*. Materials Letters, Vol.65, no.17-18, pp.2595-2597, September 2011.

[3] H. Cui, Q. Wang, and Y. Tu. *Thermally stimulated current characteristics of aged ZnO varistors under different applied voltage ratios*. Proceedings of the Asia-Pacific Power and Energy Engineering Conference (APPEEC), Wuhan, China, March 2011.

[4] C. Nahm. *Microstructure, electrical properties, and aging behaviour of ZnO-Pr6O$_{11}$-CoO-Cr$_2$O$_3$-Dy$_2$O$_3$ varistor ceramics*, Ceramics International, Vol. 37 No. 8, pp. 3049-3054, December 2011.

[5] J. Rossman, J. Nelson, and M. Droke. *Reliability and failure of porcelain highvoltage surge arresters*. International Conference on High Voltage Engineering and Application, New Orleans, USA, October 2010.

[6] C. Nahm. *Aging characteristics of ZnO-PrO$_{1.83}$-based semiconducting varistors for surge protection reliability*. Microelectronics Reliability, Vol. 54, no.11, pp. 2417-2422, November 2014.

[7] P. Bokoro and I. Jandrell. *Failure analysis of metal oxide arresters under harmonic distortion*, SAIEE Africa Research Journal, Vol. 107 No.3, pp. 167-176, September 2016.

[8] P. Bokoro and I. Jandrell. *Mean life estimation of metal oxide arresters under harmonic distortion*, Proceedings of the IEEE International Conference on Environment and Electrical Engineering (EEEIC), Florence, Italy, June 2016.

[9] IEEE 930^{TM}: *IEEE guide for the statistical analysis of electrical insulation breakdown data*, IEEE Standards 2007.

[10] A. Cimino, C. Staubach and F. Jenau. *Ageing behaviour of the insulation system used in rotating machines*, 13th IEEE International Electrical Insulation Conference (INSUCON), Birmingham, United Kingdom, May 2017.

[11] P. Preetha, M. Thomas and R. Ranjan. *Electrothermal Ageing of Epoxy Nanocomposites*, IEEE Transactions on Dielectrics and Electrical Insulation, Vol. 19, No. 6, pp. 2081 - 2089, December, 2012.

[12] J. Lee, L. Song, J. Kim, B. Lee and T. Kwon. *Aging Characteristics of Polymer Lightning Arrester by Multi-Stress Accelerated Aging Test*, lmernational Conference on Insulation and Solid Dielectrics (ICSD), Toulouse, France, July, 2004.

[13] J. Kester, D. Miller, S. Benna and B. Steinbrecher. *Multistress aging tests of polymer housed surge arresters*, IEEE Transactions on Power Delivery, Vol. 13, No. 2, pp. 446 - 452, April 1998.

[14] B. Patel, Z. Wang, J. Milanovic and P. Jarman. *Modelling Transformer Short-Circuit Reliability using Multi-Stress Accelerated Test Data*, International Conference on Probabilistic Methods applied to Power Systems, Durham, United Kingdom, July, 2014.

[15] R. Hernandez, I. Ramrez, R. Saldivar and G. Montoya.*Analysis of accelerated ageing of non-ceramic insulation equipments*, IET Generation, Transmission and Distribution, Vol. 6, no. 1, pp.59-68, January 2012.

[16] IEEE Standards C62.11 TM 2012. *Standard for metal-oxide surge arresters for AC power circuits higher than 1 kV*. IEEE power and energy society, December 2012.

[17] IEEE Standards C62.34 1996. *Performance of low-voltage surge-protective devices (secondary arresters)*. IEEE Surge Protective Devices Committee of the Power Engineering Society, December 1996.

[18] IEEE Standards C62.62 TM-2010. *Test specifications for surge-protective devices (spds) for use on the load side of the service equipment in low-voltage (1000 V and less) ac power circuits*. IEEE power and energy society, December 2010.

[19] J. He, J. Liu, J. Hu, R. Zeng and W. Long: "Non-uniform behaviour of individual grain boundaries in ZnO varistor ceramics", *Journal of the European Ceramic Society*, Vol. 31 No. 8, pp. 1451-1456, July 2011.

[20] D. Zhou, C. Zhang and S. Gong. *Degradation phenomena due to dc bias in lowvoltage ZnO varistors*. Materials Science and Engineering:B, Vol.99, no.1-3, pp. 412-415, May 2003.

[21] V. Hinrichsen. *Monitoring of high voltage metal oxide surge arresters*. 6th International Conference on Electrical Insulation, Bilbao, Spain, October 1997.

[22] M. Jaroszewski, P. Kostyla, and K. Wieczorek. *Effect of voltage harmonics content on arrester diagnostic result*. Proceedings of the International Conference on Solid Dielectrics (ICSD 2004), Toulouse, France, July 2004.

[23] R. Herrera, P. Salmeron and S. Litran. *Assessment of harmonic distortion sources in power networks with capacitor banks*. Proceedings of the 11th International Conference on Renewable Energies and Power Quality, Las Palmas de Gran Canary, Spain, April 2011.

[24] M. Balci and M. Hocaoglu. *On the validity of harmonic source detection methods and indices*, Proceedings of the 14 th International Conference on Harmonics and Quality of Power, Bergamo, Italy, September 2010.

[25] P. O'connor and A. Kleyner. *Practical Reliability*, John Wiley and Sons, UK, fifth edition, chapter 3, pp. 87-92, August 2011.

[26] J. White. *The Moments of Log-Weibull Order Statistics*, Technometrics, Vol.11, no.2, pp. 373-386, 1969.

[27] A. Yahaya, C. Yee, N. Ramli and F. Ahmad. *Determination of the best probability plotting position for predicting parameters of the weibull distribution*, International Journal of Applied Science and Technology, Vol. 2 No. 3, pp. 106-112, March 2012.

[28] R. Ross. *Graphical methods for plotting and evaluating weibull distributed data*, IEEE International conference on properties and applications of dielectric materials, Brisbane, Australia, July 1994.

[29] J. D. Campbell, A. K. S. Jardine, and J. McGlynn. *Asset management excellence: optimizing equipment life-cycle decisions*, pp. 224, CRC Press, 2016.

[30] S. Khanal1, V. Sreenivas and S. Acharya. *Accelerated Failure Time Models: An Application in the Survival of Acute Liver Failure Patients in India*, International Journal of Science and Research (IJSR), Vol.3, no.6, June 2014.

[31] S. Sutar and U. Naik-Nimbalkar.*Accelerated Failure Time Models For Load Sharing Systems*, IEEE Transactions on Reliability, Vol. 63, no. 3, pp.706 - 714, September 2014.

[32] R. Wodek. *Application of Time-to-Failure Distributions for the Modelling of Ageing Processes*, International Conference on High Voltage Engineering and Application, Shanghai, China, September 2012.

[33] D. G. Kleinbaum, and M. Klein. *Survival analysis*. Vol. 3, pp. 298. New York: Springer, 2010.

[34] S. Chiou, S. Kang and J. Yan. *Fitting Accelerated Failure Time Models in Routine Survival Analysis with R Package aftgee*, Journal of Statistical Software, Vol.61, no.11, pp. 1-23, November 2014.

[35] L. Bantis (2012). *Accelerated Failure Time (AFT) Models*. (https://www.mathworks.com/matlabcentral/fileexchange/38118-accelerated-failure-time–aft–models). MATLAB Central File Exchange. Retrieved July 2017.

[36] J. P. Klein, and M. L. Moeschberger. *Survival analysis: techniques for censored and truncated data*. pp. 399. Springer Science & Business Media, 2005.

[37] J. D. Campbell, A. K. S. Jardine, and J. McGlynn. *Asset management excellence: optimizing equipment life-cycle decisions*, pp. 224, CRC Press, 2016.